journal of the mechanical behavior of biomedical materials 150 (2024) 106299

Contents lists available at ScienceDirect

Journal of the Mechanical Behavior of Biomedical Materials

journal homepage: www.elsevier.com/locate/jmbbm

QCT-based 3D finite element modeling to assess patient-specific hip fracture risk and risk factors

Rabina Awal, Tanvir Faisal *

Department of Mechanical Engineering, University of Louisiana at Lafayette, Louisiana, USA

ARTICLE INFO

Keywords:
Hip fracture
Finite element analysis
QCT-Based FEA
Fracture risk index (FRI)
Sideways fall

ABSTRACT

Early assessment of hip fracture risk may play a critical role in designing preventive mechanisms to reduce the occurrence of hip fracture in geriatric people. The loading direction, clinical, and morphological variables play a vital role in hip fracture. Analyzing the effects of these variables helps predict fractures risk more accurately; thereby suggesting the critical variable that needs to be considered. Hence, this work considered the fall postures by varying the loading direction on the coronal plane (α) and on the transverse plane (β) along with the clinical variables—age, sex, weight, and bone mineral density, and morphological variables—femoral neck axis length, femoral neck width, femoral neck angle, and true moment arm. The strain distribution obtained via finite element analysis (FEA) shows that the angle of adduction (α) during a fall increases the risk of fracture at the greater trochanter and femoral neck, whereas with an increased angle of rotation (β) during the fall, the FRI increases by ~1.35 folds. The statistical analysis of clinical, morphological, and loading variables (α and β) delineates that the consideration of only one variable is not enough to realistically predict the possibility of fracture as the correlation between individual variables and FRI is less than 0.1, even though they are shown to be significant ($p< 0.01$). On the contrary, the correlation ($R^2= 0.48$) increases as all variables are considered, suggesting the need for considering different variables fork predicting FRI. However, the effect of each variable is different. While loading, clinical, and morphological variables are considered together, the loading direction on transverse plane (β) has high significance, and the anatomical variabilities have no significance.

1. Introduction

Hip fracture is a common injury observed in older people primarily due to osteoporosis—a condition due to which bones become weak and brittle. Osteoporotic hip fractures are associated with significant morbidity, mortality, and socioeconomic burden to both individual and the community (Pedersen et al., 2017), and thereby reducing the quality of life. The mortality rate associated with hip fractures is between 14% and 36% within the first year of hip fracture (Mundi et al., 2014). Only 50% patients recovered completely from the hip fracture, whereas 25% suffer from long-term disability (Kheirollahi and Luo, 2015). According to prior epidemiological study, the hip fracture is expected to increase to 6.62 million by the year 2050 (Dhanwal et al., 2011). The Canadian healthcare system estimated that the annual cost associated with osteoporosis treatment and related fracture was around $2.3 billion in 2010. It was projected that the worldwide cost of hip fracture-related treatment would increase to $131.5 billion by the year 2050 (Johnell, 1997). In the United States alone, approximately 300,000 hip fracture-related incidents were reported in 2014 and predicted to increase by 12% by 2030 (Krogue et al., 2020). Typically, 20% of orthopedic beds in the USA are occupied by patients with hip fractures (Bettamer, 2013). Therefore, an early assessment of hip fracture may have a huge impact on the quality of life and economy.

Clinically, *in vivo* early prediction of osteoporotic hip fracture is made by measuring Bone Mineral Density (BMD) using Dual-energy X-ray Absorptiometry (DXA) (Adams et al., 2018; Adams, 2013; Michalski et al., 2021). However, low BMD is not the only contributing factor to hip fracture, other factors such as femur geometry and fall postures may influence hip fracture (Gnudi et al., 1999; Keyak et al., 2011). Other method such as Fracture Risk Assessment Tool (FRAX) developed by the World Health Organization (WHO) in collaboration with the University of Sheffield, UK considers the population-based cohorts in Europe, North America, Asia, and Australia to predict hip fracture risk of a patient in the next ten years (El Miedany, 2020; Kanis et al., 2005). However, one of the major limitations of FRAX is not considering the fall-induced impact force, which plays an essential role in initiating hip fracture

* Corresponding author. Dept. of Mechanical Engineering, 238E Lewis St., Lafayette, LA, 70508, USA.
E-mail address: tanvir.faisal@louisiana.edu (T. Faisal).

https://doi.org/10.1016/j.jmbbm.2023.106299
Received 3 July 2023; Received in revised form 12 September 2023; Accepted 2 December 2023
Available online 10 December 2023

(Järvinen et al., 2008; Kaptoge et al., 2005). On the contrary, Hip Structural Analysis (HSA) considers the impact of fall along with 2D femoral geometry obtained via DXA. The accuracy and reliability of the HSA method primarily rely on the 2D projection of the femur bone intertwined with the proper positioning of the femur (patient) during the DXA scan (Kheirollahi and Luo, 2015).

A femur exhibits complex anatomy, and its geometry plays a significant role in hip fracture (Fajar et al., 2016). Since 3D femoral geometry plays a crucial role in predicting hip fracture, in this regard, imaging modalities such as Magnetic Resonance Imaging (MRI) and Quantitative Computed Tomography (QCT) provide more detailed information about volumetric BMD (vBMD), and volumetric bone structure as well as to occult fracture detection. However, MRI is arguably good for imaging soft tissues for better contrast. Therefore, QCT-based analysis has been considered a reliable alternative for fracture risk assessment (Muller et al., 1989; Yosibash et al., 2023). Finite Element Analysis (FEA) has been widely accepted as an effective computational tool for studying patient-specific biomechanics of bone, bone and dental implants, and many others (Chakraborty et al., 2020; Fleps et al., 2022; Liu et al., 2021; Mohammadi et al., 2021). Integrating QCT with Finite Element Analysis (QCT-based FEA) can provide a better computational framework to assess hip fracture risk more accurately in comparison with DXA-based FEA (Aldieri et al., 2020) and bone densitometry and diagnostic imaging only [15–17]. Furthermore, the QCT-based FEA is more effective as it considers vBMD, bone anatomy, and loading variability [18]. Cody et al. analyzed the reliability of QCT-based FEA for a patient-specific study and found a high correlation of 96% between the fracture load from the QCT-based FEA and experiment (Cody DD et al., 1990). Similar studies conducted by Bessho et al. and Kayak et al. showed good correlations of 97.9% and 96.2%, respectively (Beck et al., 1998; Cody DD et al., 1990; Keyak and Falkinstein, 2003). The higher correlation represents the higher accuracy of this computational model.

QCT-based FEA has been considered more reliable for its ability to accommodate the 3D geometry (Liu et al., 2020) along with the loading effect (Hennicke et al., 2022), which mainly triggers a fracture as a resultant of a fall. It is evidently reported that 90% of hip fractures occur due to a simple fall (Ford et al., 1996; Pinilla et al., 1996). Prior studies largely focused on only sideways fall at 0° (perpendicular) to the greater trochanter (Bettamer, 2013; Faisal and Luo, 2016; Kheirollahi and Luo, 2015; Munckhof and Zadpoor, 2014). However, it is a gross simplification in predicting the fracture risk as we have no control over fall orientations (postures), which necessitate assessing the effect of fall directions on the severity of hip fracture occurrences. Pinilla et al. showed that a change in loading direction from 0^o to 30^o measured from femoral neck axis on the transverse plane decreased failure load by 24%, comparable to 25 years of age-related bone loss (Pinilla et al., 1996). In a similar analysis, Ford et al. demonstrated that the variation of loading angle from 0^o to 45^o measured from the femoral neck axis reduced the structural capacity of a femur by 26%, which is again equivalent to 2-3 decades of bone loss (Ford et al., 1996). However, these analyses are limited to only varying the loading direction on the transverse plane as well as femoral strength. Following Zhang et al. (Rui Zhang et al., 2014) and Kayak et al. (Keyak and Falkinstein, 2003) who analyzed the fracture load, while varying the loading directions on different planes, we chose to vary angle (α) on the coronal plane with respect to the shaft axis and angle (β) on the transverse plane withrespect to the neck axis (Fig. 1).

Fracture load, however, may not serve as the only reliable gauge for fracture risk assessment due to the uncertainty of experiencing a load equivalent to the fracture load when a fall occurs from a standing height. Therefore, the objective of this study is to determine patient-specific Fracture Risk Index (FRI) (Awal et al., 2022; Awal and Faisal, 2021) based on patient-specific fall load, fall postures by varying loading directions (α) on coronal and (β) on transverse planes as shown in Fig. 1. We further investigated the clinical parameters—age, sex, weight, BMD; and the various morphological and anatomical variables of femur

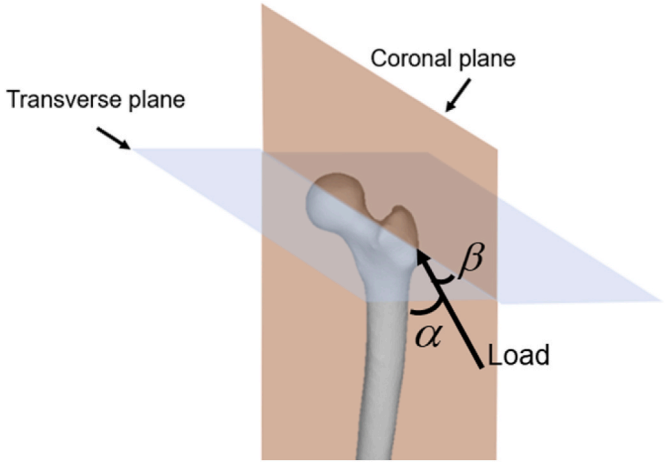

Fig. 1. Variation of loading angle α on coronal plane with respect to shaft axis of a femur and angle β on transverse plane with respect to femoral neck axis.

contributing to hip fracture. This study assessed their role via statistical significance—an essential aspect of fracture assessment that has been primarily introduced in our prior work (Awal et al., 2022). The statistical analysis aids in prioritizing the variable affecting FRI, thereby identifying critical variables to consider, while assessing the hip fracture risk.

2. Materials and methods

QCT images of 97 anonymous adults, removing all personal information, were considered in this study. The CT data set of the patients in Digital Imaging and Communications in Medicine (DICOM) format was previously obtained from the Great-West Life PET/CT Center located at the Health Science Center, Winnipeg, Canada (Faisal and Luo, 2016, 2017). The patient information in Table 1 provides a brief overview of the data set.

2.1. Image acquisition using QCT

The QCT scanned images were obtained in DICOM format by a SIEMENS S5VB40B CT scan machine (Siemens Medical Solution, Malvern, USA) with acquisition and reconstruction parameters of 120 kVp and 244 mAs, respectively, and an image matrix of 512 × 512 pixels mounted with a calcium hydroxyapatite calibration phantom (Mindways Inc., Austin, TX, USA) during the time of scanning for the correct estimation of gray value. The high-resolution data set of 1.5 mm slice thickness was used for the 3D reconstruction of femur.

2.2. Image processing and 3D femur generation

The 3D femurs were reconstructed after carefully segmenting the femur from the pelvis, tibia, fat, and muscle in 3D slicer (https://www.slicer.org/), a free open-source software for medical image processing and visualization with in-built functionalities such as thresholding,

Table 1
Characteristics of anonymous patient data set considered in this study.

	Mean (Min-Max)	Std. Dev.
Number of patients	97	-
Male	52	-
Female	45	-
Age (year)	64.93 (50-86)	8.48
Weight (kg)	83.94 (51.7-148.6)	16.72
Height (cm)	157.2 (145.3-193.2)	6.99

Std. Dev.: Standard Deviation.

smoothing, and segmentation. After applying all the image processing steps to segment the femur on each slice, the DICOM images were stacked together to get the 3D geometry (Fig. 2). In this study, we considered the proximal half of the femur with an approximate length of 220 mm measured from the superior point on the femoral head. It is to be noted that the patients-specific whole femurs are of different length. The 3D reconstructed model of proximal femur was later exported to FEA solvers in STL format for conducting FEA.

2.3. 3D FE model and mesh

The 3D femur was meshed with 4 node tetrahedral element (Awal et al., 2022; Chen et al., 2015; Lekadir et al., 2016; Luo and Yang, 2019b; Wakao et al., 2009) using HyperMesh (Altair, Michigan, USA), a high-performance finite element pre-processor. The FEA of the 3D meshed model was conducted in Ansys v19.0 (Ansys, Inc, USA). A mesh convergence study was performed with different element sizes from 4 mm up to 1 mm to achieve mesh independence. A maximum edge length of 2 mm was determined from the convergence test, achieved when the strain between the two successive iterations fell within 5%, where the strain of a predetermined point (node) was compared against the maximum element size keeping the same boundary and loading conditions. Throughout the study, all femurs were meshed with a 2 mm element size. Table 2 provides the FE modeling data.

2.4. Inhomogeneous material distributions

Although bone materials are considered anisotropic (Ashman and Van Buskirk, 1987; Keyak et al., 1997), inhomogeneous and isotropic material distributions have been shown to produce accurate results on stress, strain, and fracture load distributions, suggesting the adequacy of materials model (Ariza, 2010; E. Schileo, 2008; Keyak et al., 1997; Lotz et al., 1991). Hence, the inhomogeneous isotropic materials model was considered in this study. Each voxel of QCT images was correlated with the bone density expressed in Hounsfield Unit (HU)) (E. Schileo, 2008; Faisal and Luo, 2017). The inhomogeneous material distributions were performed by the element-wise mapping of HU via a free open-source software—Bonemat v3.0 (Fig. 2b) with creating discrete material bins (Faisal and Luo, 2016, 2017; Kheirollahi and Luo, 2015) to assign the modulus of elasticity (E). Prior experimental data established a power law between the Young's modulus and apparent density (Gislason et al., 2014). The empirical relationships in Eqs. (1)–(4) show a higher correlation with experimental data, and therefore, we adopted this relationship to assign the inhomogeneous material properties in this study (Awal et al., 2022; Awal and Faisal, 2021; Miguel Marco et al., 2019).

$$\rho_{QCT} = 0.00079114 \times HU - 0.00382144 \ \left(g \,/\, cm^3\right) \tag{1}$$

$$\rho_{ash} = 0.877 \times \rho_{QCT} + 0.0789 \ \left(g \,/\, cm^3\right) \tag{2}$$

Table 2
Mesh information.

Mesh type	3D solid, 4 node tetrahedral element (SOLID72)
Mesh size	2 mm
Average node number	18151 (ranging from 16467 to 23505)
Average element number	163360 (ranging from 148,205 to 211,554)

$$\rho_{app} = \frac{\rho_{ash}}{0.6} \ \left(g \,/\, cm^3\right) \tag{3}$$

$$E = 10500 \times \rho_{app}^{2.29} \ (MPa) \tag{4}$$

where HU represents BMD, ρ_{ash} is ash density, and E is the modulus of elasticity. Poisson's ratio was assumed to be 0.4 for all directions (Faisal and Luo, 2017).

2.5. Loading and boundary conditions

The loading configurations onto the greater trochanter were designed to accommodate a range of femur positions imitating possible sideways falling scenarios. The sideway fall postures were mimicked by simultaneously varying the orientation of the loading angle (α) on coronal plane with respect to shaft axis and angle (β) on the transverse plane with respect to neck axis as shown in Fig. 3. The limiting angles on each planes were designed considering typical fall orientations, and the most critical angle at which the maximum number of femoral fractures has been observed in prior experimental studies (Ford et al., 1996). The amount of patient-specific load, P_{fall}, to simulate the sideways fall from the standing height was calculated as per Eq. (5) (Robinovitch et al., 1991; Yoshikawa et al., 1994).

$$P_{fall} = 8.25 \times w \times \left(\frac{h}{170}\right)^{1/2} \ (N) \tag{5}$$

where w and h are the weight and height of a patient, respectively.

In the FE simulation, 9 different sideways fall conditions were simulated varying the angle of adduction (α) and the angle of rotation (β) as shown in Fig. 4a. Each sideways fall represents a different combination of loading directions on coronal plane, $\alpha \in [0^o, 30^o]$ with 15^o interval and on transverse plane, $\beta \in [-15^o, 15^o]$, with an interval of 15^o, as shown in Table 3.

For each loading scenario, the distal end of the proximal femur was fixed in all directions, except the rotational degree of freedom along the y-axis, representing the pivot joint (knee) at the distal end of a femur (Altai et al., 2019; Yano et al., 2022). The translational degrees of freedom at the femur head were fixed, allowing it to rotate in x, y, and z directions to mimic the ball and socket joint between the femur head and acetabulum, and the load was applied on the greater trochanter (Fig. 4b).

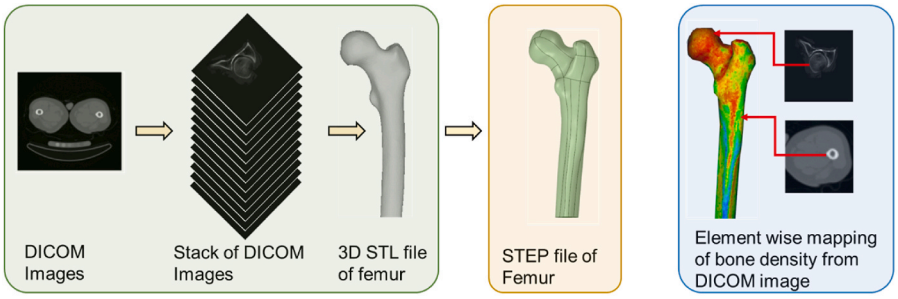

Fig. 2. (a) An overview of 3D reconstruction of proximal femur from QCT image data set; (b) Element-wise mapping of inhomogeneous material distributions in femur using Bonemat v3.0.

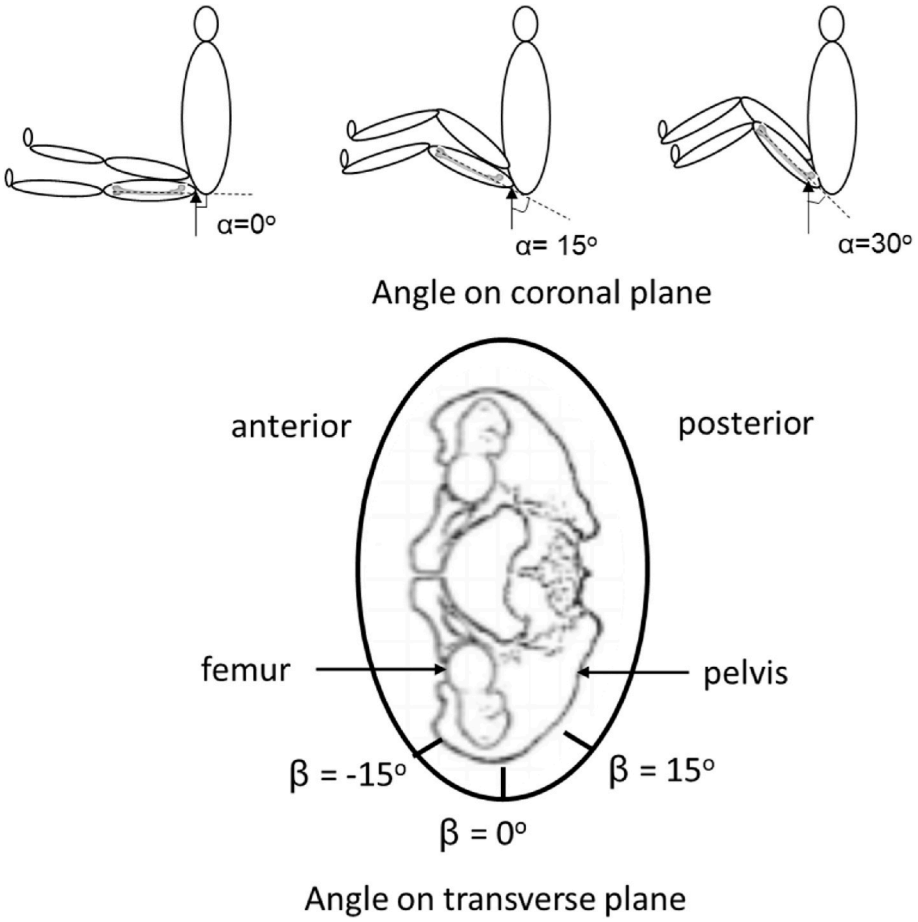

Fig. 3. A schematic representation of the variation of sideways fall on coronal plane (top) denoted by angle (α) and on transverse plane denoted by angle (β).

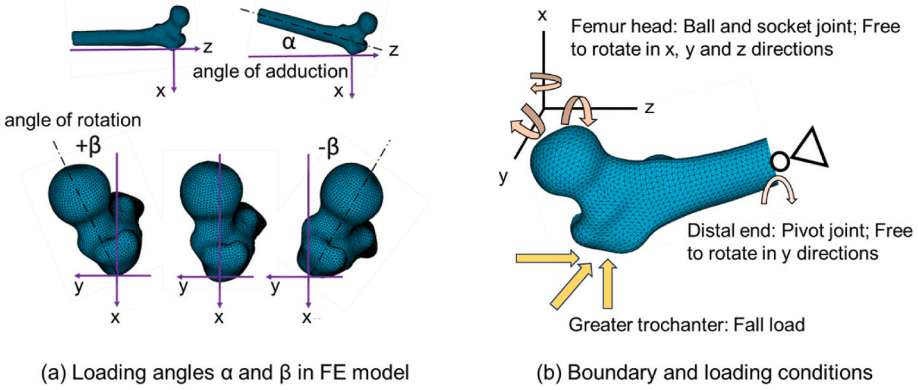

Fig. 4. (a) Representation of loading angles α and β on coronal and transverse planes, respectively, and (b) Boundary and loading conditions at the distal end, femur head, and greater trochanter of a femur during FEA.

2.6. Failure criteria

In this study, a linear FEA was performed as the femur bone behaves linearly elastic up to failure (Cristofolini et al., 2007; Grassi et al., 2012; Juszczyk et al., 2011). A femur also exhibits brittle behavior that is better represented by the maximum stress-strain criteria rather than the magnitude of stress and strain (von Mises stress/strain criteria) (Cristofolini et al., 2007; Doblaré et al., 2004). Schileo et al. (E. Schileo, 2008) and other studies (Ali et al., 2014; Marco et al., 2019; Testi et al., 2002) showed that principal strain-based FEA could more accurately estimate fracture risk. Therefore, we have adopted the maximum principal strain-based criteria to determine the FRIs, which are defined based on the absolute maximum tensile (1st principal) and compressive (3rd principal) strains (Bayraktar et al., 2004; E. Schileo, 2008) as follows.

$$FRI = \frac{\varepsilon^{T}_{\max}}{0.0073} \tag{6}$$

$$FRI = \frac{\left|\varepsilon^{c}_{\max}\right|}{0.0104} \tag{7}$$

where $\varepsilon^{T}_{\max}$ and $\varepsilon^{c}_{\max}$ are the maximum principal strain in tension and

Table 3
Sideways fall configurations modeled in QCT-based FEA to mimic possible sideways fall orientations.

Sideways fall cases	α (degree)	β (degree)
αβ_0/-15	0	-15
αβ_0/0	0	0
αβ_0/15	0	15
αβ_15/-15	15	-15
αβ_15/0	15	0
αβ_15/15	15	15
αβ_30/-15	30	-15
αβ_30/0	30	0
αβ_30/15	30	15

compression, respectively.

2.7. Clinical and morphological variables for statistical significance

Clinical parameters such as sex, age, weight, height, and bone mineral density (BMD) are primarily attributed to hip fracture as shown in prior studies (Fajar et al., 2018; Ford et al., 1996; Keller, 1994; Marks et al., 2003; Pinilla et al., 1996). One of the primary causes of femoral fracture is osteoporosis—loss of BMD. The maximum BMD in a femur is typically observed in adults between the age of 25 and 29 years (Szulc et al., 2000), and the BMD starts decreasing after that. On average, there is a 13% to 18% loss in bone mass from peak BMD to age 80 (Szulc et al., 2000). In addition, the average BMD and rate of BMD loss differ between male and female. A study conducted on a cohort of 36 healthy men and women of the same age group shows that men have an 8% higher BMD than women (Nieves et al., 2005). Over a four-year interval, loss in BMD for men is 0.2% to 3.6%, and for women, it is 3.4% to 4.8%, indicating that the BMD of women is deteriorating at a higher rate (Jones et al., 1994). A Survey conducted by the National Health and Nutrition Examination Survey (NHANSE) from 1988 to 1994 reported that the presence of osteoporosis in female is 16% to 56%, whereas for men is 2% to 18% (Cha et al., 2022). In addition, our prior study shows that the height and weight of a patient have a significant correlation with hip fracture (Awal et al., 2022). Hence, sex, age, weight, height, and BMD have been considered as the relevant clinical parameters.

Hip fractures are also attributed to femur morphology and may be predicted by simple measurement of the femoral geometry, and geometric risk factors predict hip fractures regardless of BMD (Faulkner et al., 1993). For example, an increase of the femoral neck width (FNW) plays an important role as a risk factor for fracture independently of BMD (Han and Hahn, 2016). Fajar et al. showed the significance of FNW, femur neck axis length (FNAL), femur neck angle (FNA) and femur neck arm/true moment arm (TMA) (Fajar et al., 2016) on hip fracture. A number of prior studies on cross-sectional area, FNW, and FNAL have been reported, but different results have been found depending on race, sex, and age (Awal et al., 2022; Beck, 2007; Kim et al., 2011; LaCroix et al., 2010; Yoshikawa et al., 1994).

It is evident that both clinical and morphological variables play important roles in hip fracture and are expected to have different levels of effect on FRI (Awal et al., 2022). Clinical variables—age, sex, weight, and BMD were obtained from the DICOM metadata and the image of each patient. The height of the patient was derived based on the following empirical equations obtained from the study done by Wod et al. (Wod, 2008)

$$Height_{men} = 2.610 \times femur + 44.201 \quad (8)$$

$$Height_{women} = 2.019 \times femur + 67.579 \quad (9)$$

Morphological variables were obtained from the 2D projection of the FE meshed model of patients' femurs on the coronal plane. With reference to Fig. 5, AB represents FNAL, obtained by noting the coordinates of the nodes of the outer margin on the femur head and greater trochanter such that it passes through the middle of the femoral neck; CD represents the FNW, calculated between the outer coordinates on the minimum neck region; and ED represents the TMA, the horizontal component of FNAL on transverse plane (Gong et al., 2012). FNA is the intersection between the proximal femoral shaft axis and the femoral neck axis and is represented by θ (Fajar et al., 2018).

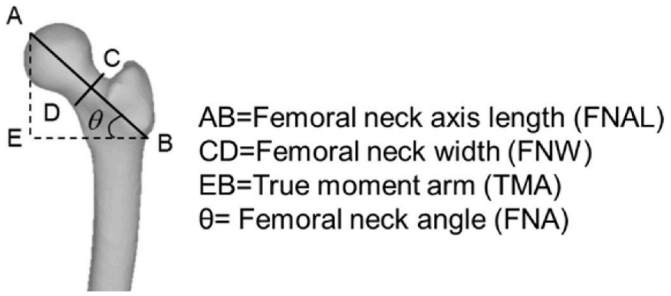

Fig. 5. A proximal femur morphology and its different geometric parameters that were considered in this study.

3. Results

The strain distribution in femurs was obtained for different loading cases. Fig. 6 shows von Mises strain, 1st principal strain (tensile strain), and 3rd principal strain (compressive strain) for the loading condition $\alpha\beta$_0/0. This loading condition is the base sideways fall loading direction along which the FEA was previously validated with maximum von Mises strain (Awal et al., 2022; Awal and Faisal, 2021). It is evident that higher strain is observed in the proximal end compared to femur diaphysis (Fig. 6b and c). It has been further observed that tensile strain is higher on the inferior surface of the proximal end, whereas the compressive strain is higher on the superior side of the proximal region.

Fig. 7 depicts the variation of 1st principal (tensile) strains with respect to different fall loading cases. It illustrates that the strain at the femoral neck region is always higher irrespective of loading cases. As the angle α on the coronal plane varies from 0^o to 30^o, the higher strain is observed at the trochanteric regions in addition to femoral neck region (Fig. 7). However, the variation of angle β on transverse plane from -15^o to 15^o with a specific angle of α plays a non-sgnifiant role in generating region-wide higher strain, implying that the region of strain distribution is independent of the loading angle β on the transverse plane.

FRI for each loading case will help analyze the fracture tendency with respect to loading directions. The violin plots in Fig. 8 show the distribution of FRI for each loading case as a continuous approximation of the Probability Density Function (PDF), computed using Kernel Density Estimation (KDE). The wider regions of the density plot indicate FRI values that occur more frequently, and the narrower sections represent a lower probability, indicating FRI values that occur less frequently. The violin plot uses KDE to compute an empirical distribution of sample data, and therefore, it better reveals the information contained in the sample and more convincingly suggests multimodality. Distributional differences of the FRI of the femurs of different loading cases are exhibited in the violin plots, displaying each dataset's KDE (smoothed histograms). They are helpful in comparing the groups. We see a trend of multimodality when the angle β is 15^o.

The violin plots further demonstrate that with increasing β from -15^o to 15^o, the mean FRI increase from 0.83 to 1.117 when α is fixed at 0^o, 0.83 to 1.13 at α equals to 15^o, and 0.76 to 1.06 when α is restricted to 30^o. Overall, the FRI is ~1.35 times greater at 15^o as compared with -15^o. The result shows that FRI increases significantly with increasing β on the transverse plan, while the variation is minimal with the variation of angle α on the coronal plane. Furthermore, the mean FRI values increases with increasing β on the transverse plane as shown by the red dotted line in Fig. 8. This delineates the fact that FRI depends more on

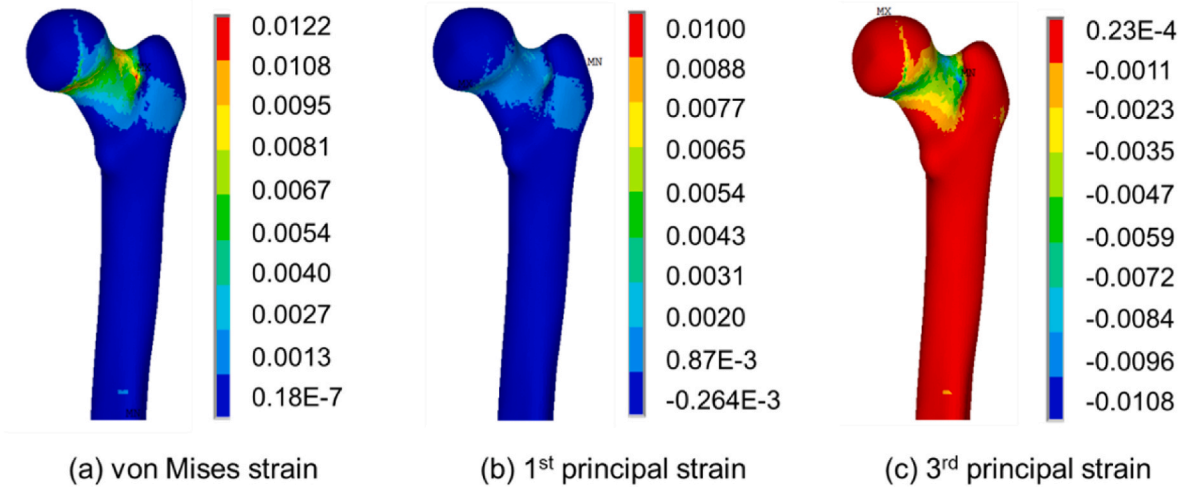

Fig. 6. Typical strain distributions in sideways fall, $\alpha\beta\_0/0$, obtained via FEA. (a) von Mises strain (b) 1st principal (Tensile) strain and (c) 3rd principal (Compressive) strain.

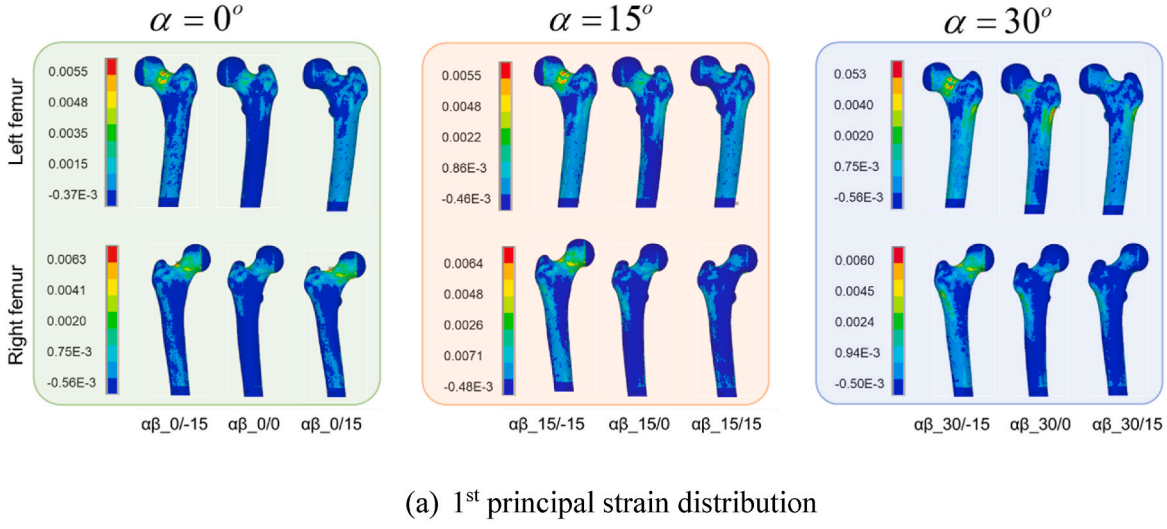

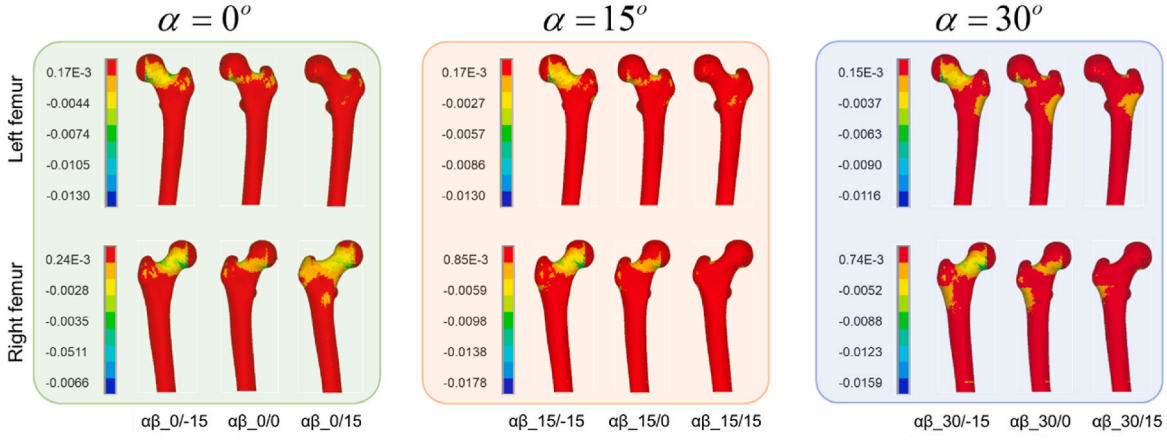

Fig. 7. 1st principal strain (a) and 3rd principal strain (b) distributions due to sideways fall at different loading orientations represented by the variation of loading angle α measured from femur shaft on coronal plane and angle β measured from neck axis length on transverse plane.

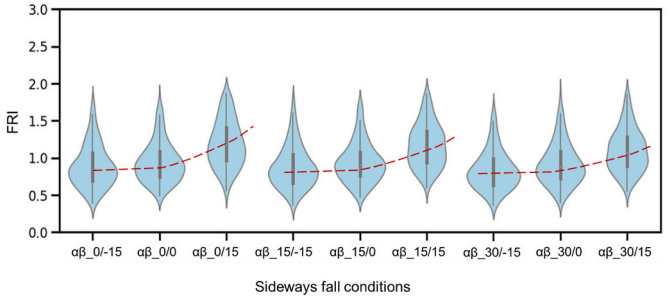

Fig. 8. Violin plots showing the distributions of FRI at different sideways fall conditions obtained by varying loading angles α and β on coronal and transeverse planes, respectively. The red dotted line shows the increasing trend of mean FRI with increasing β on transverse plane only.

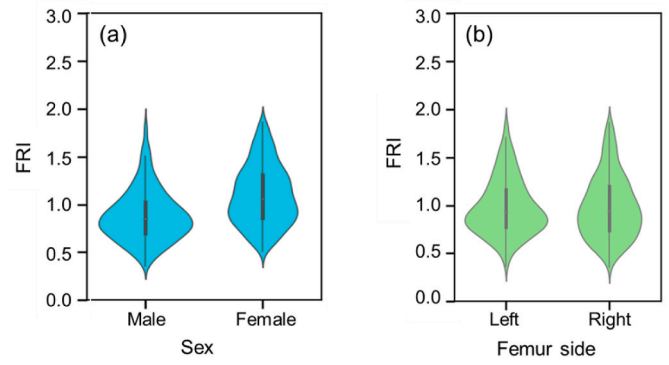

Fig. 9. Comparison of sex-dependent (a) and bilateral (b) FRI distributions.

angle β than on angle α.

The violin plots in Fig. 9 show the sex-dependent and bilateral variations of FRI and its distribution. The mean FRIs for male and female were 0.84 and 1.05, respectively, indicating that females are more susceptible to fracture. The sex-dependent FRI distribution of male is normal, whereas the distribution of female tends to be bimodal (Fig. 9a). On the other hand, the mean FRI for both the left and right femurs is nearly equal and approximately 0.98, showing that FRI is independent of femur sides. However, the FRI distributions of right femur also show a bimodal trend (Fig. 9b).

The role of clinical and morphological variables has been shown in Figs. 10 and 11, respectively, where the correlation of age, weight, BMD, FNAL, FNA, FNW, and TMA with FRI has been demonstrated. The solid (black) line in the scatter plot represents the average distribution of the variables. Clinically, FRI increases with age and weight but decreases with an increase in BMD (Fig. 11). Morphologically, FRI increases with FNA but decreases with an increase in FNAL, FNW, and TMA.

In addition to structurally determined FRI, a statistical analysis of the effect of loading direction along with the clinical and morphological variables was done in the statistical software JMP® Pro 15 (SAS Institute Inc, USA). The significance of individual variables on FRI was obtained at a significant level of 0.01. $p \leq 0.01$ shows a significant effect on FRI, and $p > 0.01$ indicates no effect of variables on FRI. The *Pearson Coefficient* (R^2) shows the degree of dependency or the extent to which the variable explains the FRI. Table 4 shows the significance and the correlation of variables.

P-values for α ($p = 0.0087$, $R^2 = 0.05$), β ($p < 0.0001$, $R^2 = 0.154$), sex ($p < 0.0001$, $R^2 = 0.117$), age ($p < 0.0001$, $R^2 = 0.014$), weight ($p < 0.0001$, $R^2 = 0.017$), BMD ($p < 0.000$, $R^2 = 0.091$), FNAL ($p < 0.0001$, $R^2 = 0.024$), FNW ($p < 0.0001$, $R^2 = 0.02$), FNA ($p < 0.0001$, $R^2 = 0.01$), and TMA ($p < 0.0001$, $R^2 = 0.033$) show the statistical significance of these variables on FRI but weak correlation. Among the variables analyzed, only the femur side ($p = 0.8220$, $R^2 = 0.0003$) was found to be insignificant.

The correlation obtained in Table 4 is the extent to which an individual parameter alone defines the variability of FRI. Analysis was further done to analyze the variability of FRI in the presence of all (or other) variables. It was found that the correlation between all the variables and FRI increased to 0.482 with the significance of $p < 0.0001$. The effect of each variable in the presence of other variables has been shown in Table 5. It shows that the effect of β is comparatively higher than that of other variables, and there is no significant effect of FNA, FNAL, TMA, and (femur) side in the presence of other variables.

4. Discussion

The overarching goal of this study is to assess hip fracture risk in terms of FRI in a more comprehensive manner by widely accepted computational modeling approach—FEA, mimicking fall postures via varying the loading directions on coronal and transverse planes. In addition to clinical parameters and 3D bone morphology, loading direction is an important determinant influencing the FRI. However, the FRI calculated through FEA mainly provides an overall failure probability from the mechanistic standpoint without identifying/ranking the underlying factors. Therefore, statistical modeling has been conducted to identify the effect of variables on fracture risk assessment (Awal et al., 2022).

From the results, we see that strain is always higher at the proximal end during sideways fall conditions, irrespective of loading direction (Figs. 6 and 7). It signifies that the proximal region, including the femoral neck and trochanteric regions, are the most critical regions compared to the femoral shaft region. The worldwide femoral shaft and proximal fracture incidents also support this computational finding. The femoral shaft fracture is between 10 and 21 per 100,000 people per year, whereas the proximal fracture is 769.7 per 100,000 people per year (Denisiuk and Afsari, 2022; Longo et al., 2022). As per bone morphology, spongy and less stiff trabecular bone in the proximal region makes it weak and prone to fracture. On the contrary, compact, and stiff cortical bone in the femoral shaft region makes it strong and less vulnerable. Therefore, the proximal femur is the primary region of interest (Bergot et al., 2002; Gnudi et al., 1999; Orwoll et al., 2009) for

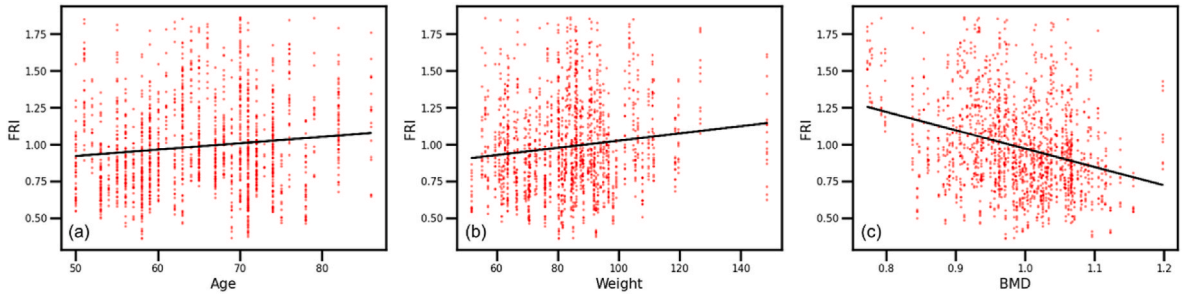

Fig. 10. Variation of FRI with respect to clinical variables—age (a), weight (b), BMD (c).

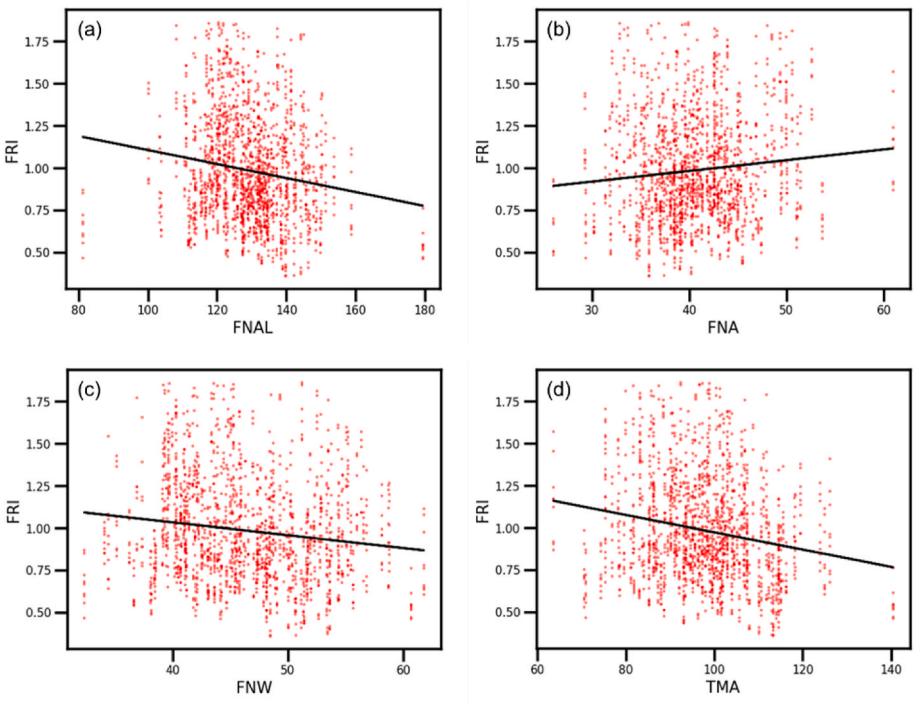

Fig. 11. Variation of FRI with respect to morphological variables—FNAL (a), FNA(b), FNW (c), and TMA (d).

Table 4
Statistical analysis of the variables affecting FRI to analyze their significance and extent of the effect on FRI.

Variables	*P-value*	Correlation (R^2)
α	0.0087	0.005
β	<0.0001	0.154
Sex	<0.0001	0.117
Age	<0.0001	0.014
Weight	<0.0001	0.017
BMD	<0.0001	0.091
FNAL	<0.0001	0.024
FNW	<0.0001	0.020
FNA	<0.0001	0.010
TMA	<0.0001	0.033
Side	0.8229	0.00003

Table 5
Effect summary of variables on FRI.

Source	LogWorth	PValue
β	101.462	0.00000
Weight	55.795	0.00000
BMD	54.103	0.00000
Sex	29.143	0.00000
Age	14.837	0.00000
α	4.519	0.00003
FNW	2.375	0.00422
FNA	1.609	0.02463
FNAL	1.568	0.02702
TMA	0.828	0.14847
Side	0.034	0.92404

fracture risk assessment.

The strain distribution patterns at different sideways fall cases (Fig. 7) demonstrate that the region of a femoral fracture depends primarily on angle of adduction (α)—the angle between the femur shaft axis and loading direction on the coronal plane. With the increase of the adduction angle (α), the risk of intertrochanteric fracture increases. On the contrary, the angle of rotation (β)—the angle between the femur neck axis and loading direction on transverse plane (β) does not affect the region of fracture as long as α remains the same. This indeed gives a notable insight into the loading effect that the fracture location is primarily influenced by the angle of adduction during a fall on the coronal plane.

The fracture risk, on the other hand, largely depends on the angle of rotation (β) on transverse plane irrespective of the angle of adduction on coronal plane (α). The increase in mean FRI from the minimum to the maximum as β changes from -15° to 15° (Fig. 8) implies that the femur is more vulnerable to fracture when a fall occurs more along the posterolateral direction than in the anterolateral direction. This observation is also supported by prior studies showing the dependency of femoral fracture on transverse plane. Ford et al. showed that the structural capacity of the femur was decreased by 12% with the change of angles from 0° to 15° (Ford et al., 1996). Galliker et al. concludes that the number of femoral fractures is higher at posterolateral 15°, and the number of fracture decreases with increasing posterolateral loading direction suggesting more critical loading direction on transverse plane (Galliker et al., 2022). A similar result has been observed statistically in the present study. The statistical analysis shows the significance of α ($p = 0.0087$) on FRI as *p-value* is less than 0.01. It implies that an FRI changes with α, but the R^2 (0.005) value shows a lower degree to which FRI changes with respect to α. The *p-value* (<0.0001) of β shows the significance of β on FRI and resembles that the changes in β influence the FRI value, and the R^2 (0.154) shows higher dependency of FRI on β compared with α.

Clinically, women are more susceptible to fracture than men because of bone loss, especially after 50 years due to menopause. A prior study conducted in 2004 determined 99,000 and 93,000 hip fractures in feamle and male, respectively (Orwig et al., 2006). This study also substantiated the clinical observations (Fig. 9a). However, the equal FRI of left and right femurs indicate bone loss in general is similar and equally affects the femurs—a trend observed in general. Furthermore, we also observe that the fracture probability increases with age (Fig. 10a), which is also evident since the rate of bone resorption

increases in comparison to the rate of bone formation as we grow old. However, the low correlation between age and FRI also resembles that age is not the only determinant affecting hip fracture. Similarly, the positive slope and low correlation between weight and FRI (Fig. 10b) indicate the role of weight in fracture risk assessment. This finding can be linked with obesity, which may cause physiological changes in bone properties and increase the impact load due to high weight. However, large muscle volume may provide some cushioning effect during a fall, which may subdue the intensity of impact force as well. Hip fracture risk is expected to increase with a decrease in BMD (Fig. 10c). Low BMD is related to low bone mass or loss of bone quality, indicating osteoporosis. This observation also aligns with the clinical findings that osteoporotic patients have a high hip fracture incidence (Mai et al., 2019).

The negative slopes obtained in the scatter plots between FNAL and FRI, FNW and FRI, and TMA and FRI (Fig. 11a, c, d) show the correlation of hip fracture with bone morphology such that the probability of hip fracture increases with decrease in neck axis length, femur neck width, and moment arm. It suggests that a person with a larger cross-section area of the femur neck is less susceptible to fracture. Similarly, a person with longer femur neck length is less likely to have a hip fracture. However, the positive slope obtained between FNA and FRI (Fig. 11b) depicts a person with a larger neck-shaft angle has a higher probability of hip fracture than one with a smaller neck-shaft angle. The current study was conducted with only 97 patients and no information was available if and how many patients were clinically diagnosed with osteoporosis, which is highly correlated with hip fracture. Since the data was provided without patient health conditions, the analysis was done as a single cohort. Such variations can be minimized if the analysis can be done with a larger dataset having a cohort of control patients (healthy patients without osteoporosis) and a cohort of clinically diagnosed osteoporotic patients.

Although there are relationships among the considered variables and FRI, the R^2 (<0.1) between each variable and FRI, (Table 4), shows that a single parameter is not enough to predict the incidence of hip fracture. On the contrary, the R^2 (0.48) obtained considering all variable increase the interpretability of FRI. This finding implies that all the variables cumulatively increase hip fracture risk, but existing clinical diagnosis/prediction has been made on BMD (Altai et al., 2019; Dall'Ara et al., 2016; Munckhof and Zadpoor, 2014) only. It is evident from this analysis that the mechanistic prediction via FEA is not sufficient and parameters such as weight, age, and sex of a patient should be considered in assessing the hip fracture risk. Furthermore, the effect of all the variables on predicting hip fracture risk is also not the same; the clinical variables have been found to be more significant than the morphological (anatomical) ones.

Although this study represents a comprehensive analysis of fracture risk assessment, there are some limitations in this study. The loading and boundary conditions in this QCT-based FEA is the replication of prior *ex vivo* experiment with femurs only, excluding muscles and fats (Choi et al., 2015). This boundary condition has been explicitly used in several *ex vivo* experiments to investigate the femoral strength, which is associated with the possibility of hip fracture (Dinçel VE et al., 2008; Kyle K. Nishiyama et al., 2007; Luo and Yang, 2019a; Masahiko Bessho et al., 2009; Yang et al., 2018). Ignoring the effect of muscle and fat is apparently a limiting assumption since muscle and fat can absorb a fraction of impact energy causing femoral fracture. Although fracture risk is highly correlated with a femur's strength, the fracture risk estimation ignoring muscle might provide a higher risk than the actual scenario, but this will make the diagnosis more conservative to prevent fracture. The other potential sources of error in FEA include the stress concentration, element type, and element aspect ratio. These sources of error were minimized in this study via monitoring element quality such that the aspect ratio of element is limited to 5. The femurs in this analysis were modeled with smoothed surface that eliminated stress concentration. However, a patient-specific femur may have stress concentration due to its complex geometry and bone deformity. Furthermore, the optimum size of element in FEA was obtained after mesh convergence test and a higher mesh refinement has been implemented to increase the number of elements to avoid over stiffness of the 4 node tetrahedral element. In addition, to reduce the computation cost, the interval for angle α and β was set to 15^o, which can be decreased to get more data points for more accurate statistical analysis to reduce bias, if there is any.

5. Conclusion

The aim of this study was to analyze the effect of loading directions, bone morphology, and clinical variables on FRI obtained via QCT-based FEA. To investigate the effect of fall orientation and postures, the loading direction in terms of angle α and β was varied on coronal and transverse planes, respectively. The strain distributions at different sideways fall cases show that with changing the angle of adduction (α) during fall from 0^o to 30^o, the risk of fracture increases at greater trochanter and femur neck; however, as the angle of rotation (β) increases during a fall from -15^o to 15^o, the FRI increase by ~1.35 folds. The statistical analyses of clinical, morphological, and loading variables (α and β) show that the consideration of single variable is not enough to predict the possibility of fracture as the correlation (R^2) between an individual variable and FRI is less than 0.1 even though the $p-values$ show significant ($p<0.01$). On the contrary, the correlation ($R^2=0.48$) increases while all the variables are considered. The effect test shows that the loading direction, especially on transverse plane (β), is more critical than the other variables, while cumulatively considering all the variables.

The prediction of hip fracture could aid in enhancing the quality of life by recommending proper medications and preventive measures. This analysis can be used as a primary assessment tool to design effective clinical intervention to prevent fracture. Studies done in cohort of 51 elderly women has found that by increasing the level of vitamin K, the possibility of hip fracture decreases (Hodges et al., 1993). Also, early prediction of hip fracture helps reducing the possibility of hip fracture by using hip protector. It was found that hip protector decrease the probability of hip fracture from 19.8% to 2% (Harada et al., 2001). However, the present analysis has been done based on only one cohort of patients of certain geographic locations. In future, this study can be extended to conduct on patients with different geographic locations, race, ethnicity, older than 70 years of age, and most importantly patients with clinically identified osteoporosis.

Funding

No funding was available for this study.

Data and materials availability

The datasets presented during the current study are not publicly available due to privacy and ethical restrictions but might be available on reasonable request from the corresponding author.

CRediT authorship contribution statement

Rabina Awal: Writing – original draft, Methodology, Investigation, Formal analysis. **Tanvir Faisal:** Writing – review & editing, Supervision, Project administration, Formal analysis, Conceptualization.

Declaration of competing interest

The authors declare that they have no known competing financial interests or personal relationships that could have appeared to influence the work reported in this paper.

Data availability

Data will be made available on request.

Acknowledgments

The authors greatly acknowledge undergraduate research student, Sarah Doll of Mechanical Engineering at UL Lafayette for assisting in 3D femur reconstruction.

References

Adams, J.E., 2013. Advances in bone imaging for osteoporosis. Nat. Rev. Endocrinol. 9, 28.
Adams, A.L., Fischer, H., Kopperdahl, D.L., Lee, D.C., Black, D.M., Bouxsein, M.L., Fatemi, S., Khosla, S., Orwoll, E.S., Siris, E.S., Keaveny, T.M., 2018. Osteoporosis and hip fracture risk from routine computed tomography scans: the fracture, osteoporosis, and CT utilization study (FOCUS), 33, 1291–1301.
Aldieri, A., Terzini, M., Audenino, A.L., Bignardi, C., Morbiducci, U., 2020. Combining shape and intensity dxa-based statistical approaches for osteoporotic HIP fracture risk assessment. Comput. Biol. Med. 127, 104093.
Ali, A.A., Cristofolini, L., Schileo, E., Hu, H., Taddei, F., Kim, R.H., Rullkoetter, P.J., Laz, P.J., 2014. Specimen-specific modeling of hip fracture pattern and repair, 47, 536–543.
Altai, Z., Qasim, M., Li, X., Viceconti, M., 2019. The effect of boundary and loading conditions on patient classification using finite element predicted risk of fracture. Clin. BioMech. 68, 137–143.
Ariza, O.R., 2010. A Novel Approach to Finite Element Analysis of Hip Fractures Due to Sideways Falls, Mechanical Engineering. University of Waterloo.
Ashman, A.B., Van Buskirk, W.C., 1987. The elastic properties of a human mandible, 1, 64–67.
Awal, R., Faisal, T.R., 2021. Multiple regression analysis of hip fracture risk assessment via finite element analysis. Journal of Engineering and Science in Medical Diagnostics and Therapy 4, 011006.
Awal, R., Ben Hmida, J., Luo, Y., Faisal, T., 2022. Study of the significance of parameters and their interaction on assessing femoral fracture risk by quantitative statistical analysis. Med. Biol. Eng. Comput. 60, 843–854.
Bayraktar, H.H., Morgan, E.F., Niebur, G.L., Morris, G.E., Wong, E.K., Keaveny, T.M., 2004. Comparison of the elastic and yield properties of human femoral trabecular and cortical bone tissue. J. Biomech. 37, 27–35.
Beck, T.J., 2007. Extending DXA beyond bone mineral density: understanding hip structure analysis. Curr. Osteoporos. Rep. 5, 49–55.
Beck, T.J., Mourtada, F.A., Ruff, C.B., Scott, W.W., Kao, G., 1998. Experimental testing of a DEXA-derived curved beam model of the proximal femur. J. Orthop. Res. 16, 394–398.
Bergot, C., Bousson, V., Meunier, A., Laval-Jeantet, M., Laredo, J., 2002. Hip fracture risk and proximal femur geometry from DXA scans. Osteoporos. Int. 13, 542–550.
Bettamer, A., 2013. Prediction of Proximal Femur Fracture: Finite Element Modeling Based on Mechanical Damage and Experimental Validation.
Cha, Y., Kim, J.T., Park, C.H., Kim, J.W., Lee, S.Y., Yoo, J.I., 2022. Artificial intelligence and machine learning on diagnosis and classification of hip fracture: systematic review. J. Orthop. Surg. Res. 17, 520.
Chakraborty, A., Datta, P., Majumder, S., Mondal, S.C., Roychowdhury, A., 2020. Finite element and experimental analysis to select patient's bone condition specific porous dental implant, fabricated using additive manufacturing. Comput. Biol. Med. 124, 103839.
Chen, G., Wu, F., Liu, Z., Yang, K., Cui, F., 2015. Comparisons of node-based and element-based approaches of assigning bone material properties onto subject-specific finite element models. Med. Eng. Phys. 37, 808–812.
Choi, W.J., Cripton, P.A., Robinovitch, S.N., 2015. Effects of hip abductor muscle forces and knee boundary conditions on femoral neck stresses during simulated falls. Osteoporos Int. 26, 291–301.
Cody DD, G.G., Hou, F.J., Spencer, H.J., Goldstein, S.A., Fyhrie, D.P., 1990. Femoral strength is better predicted by finite element models than QCT and DXA. J. Biomech. 32, 1013–1020.
Cristofolini, L., Juszczyk, M., Martelli, S., Taddei, F., Viceconti, M., 2007. In vitro replication of spontaneous fractures of the proximal human femur. J. Biomech. 40, 2837–2845.
Dall'Ara, E., Eastell, R., Viceconti, M., Pahr, D., Yang, L., 2016. Experimental validation of DXA-based finite element models for prediction of femoral strength. J. Mech. Behav. Biomed. Mater. 63, 17–25.
Denisiuk, M., Afsari, A., 2022. Femoral Shaft Fractures, StatPearls [Internet]. StatPearls Publishing.
Dhanwal, D.K., Dennison, E.M., Harvey, N.C., Cooper, C., 2011. Epidemiology of hip fracture: worldwide geographic variation. Indian J. Orthop. 45, 15–22.
Dinçel VE, S.M., Sepici, V., Cavuşoğlu, T., Sepici, B., 2008. The association of proximal femur geometry with hip fracture risk. Clin. Anat. 21, 575–580.
Doblaré, M., Garcıa, J., Gómez, M., 2004. Modelling bone tissue fracture and healing: a review. Eng. Fract. Mech. 71, 1809–1840.
El Miedany, Y., 2020. FRAX: re-adjust or re-think. Arch. Osteoporosis 15, 1–8.
Faisal, T.R., Luo, Y., 2016. Study of stress variations in single-stance and sideways fall using image-based finite element analysis. Bio Med. Mater. Eng. 27, 1–14.
Faisal, T.R., Luo, Y., 2017. Study of the variations of fall induced hip fracture risk between right and left femurs using CT-based FEA. Biomed. Eng. Online 16, 116.
Fajar, J.K., Rusydi, R., Rahman, S., Alam, A.I.N., Azharuddin, A., 2016. Hip geometry to predict femoral neck fracture: only neck width has significant association. Apollo 13, 213–219.
Fajar, J.K., Taufan, T., Syarif, M., Azharuddin, A., 2018. Hip geometry and femoral neck fractures: a meta-analysis. Journal of orthopaedic translation 13, 1–6.
Faulkner, K.G., Cummings, S.R., Black, D., Palermo, L., Glüer, C.C., Genant, H.K., 1993. Simple measurement of femoral geometry predicts hip fracture: the study of osteoporotic fractures. J. Bone Miner. Res. 8, 1211–1217.
Fleps, I., Pálsson, H., Baker, A., Enns-Bray, W., Bahaloo, H., Danner, M., Singh, N.B., Taylor, W.R., Sigurdsson, S., Gudnason, V.J.B., 2022. Finite element derived femoral strength is a better predictor of hip fracture risk than aBMD in the AGES Reykjavik study cohort, 154, 116219.
Ford, C.M., Keaveny, T.M., Hayes, W.C., 1996. The effect of impact direction on the structural capacity of the proximal femur during falls. J. Bone Miner. Res. 11, 377–383, 372.
Galliker, E.S., Laing, A.C., Ferguson, S.J., Helgason, B., Fleps, I., 2022. The influence of fall direction and hip protector on fracture risk: FE model predictions driven by experimental data. Ann. Biomed. Eng. 50, 278–290.
Gislason, M.K., Ingvarsson, P., Gargiulo, P., Yngvason, S., Guðmundsdóttir, V., Knútsdóttir, S., Helgason, þ., 2014. Finite element modelling of the femur bone of a subject suffering from motor neuron lesion subjected to electrical stimulation. European journal of translational myology 24.
Gnudi, S., Ripamonti, C., Gualtieri, G., Malavolta, N., 1999. Geometry of proximal femur in the prediction of hip fracture in osteoporotic women. Br. J. Radiol. 72, 729–733.
Gong, H., Zhang, M., Fan, Y., Kwok, W.L., Leung, P.C., 2012. Relationships between femoral strength evaluated by nonlinear finite element analysis and BMD, material distribution and geometric morphology. Ann. Biomed. Eng. 40, 1575–1595.
Grassi, L., Schileo, E., Taddei, F., Zani, L., Juszczyk, M., Cristofolini, L., Viceconti, M., 2012. Accuracy of finite element predictions in sideways load configurations for the proximal human femur. J. Biomech. 45, 394–399.
Han, J., Hahn, M.H., 2016. Proximal femoral geometry as fracture risk factor in female patients with osteoporotic hip fracture. J. Bone Metabol. 23, 175–182.
Harada, A., Mizuno, M., Takemura, M., Tokuda, H., Okuizumi, H., Niino, N., 2001. Hip fracture prevention trial using hip protectors in Japanese nursing homes. Osteoporosis Int. 12, 215–221.
Hennicke, N., Saemann, M., Kluess, D., Bader, R., Sander, M., 2022. Subject specific finite element modelling of periprosthetic femoral fractures in different load cases. J. Mech. Behav. Biomed. Mater. 126, 105059.
Hodges, S.J., Akesson, K., Vergnaud, P., Obrant, K., Delmas, P.D., 1993. Circulating levels of vitamins K1 and K2 decreased in elderly women with hip fracture. J. Bone Miner. Res. 8, 1241–1245.
Järvinen, T.L.N., Sievänen, H., Khan, K.M., Heinonen, A., Kannus, P., 2008. Shifting the focus in fracture prevention from osteoporosis to falls. BMJ 336, 124–126.
Johnell, O., 1997. The socioeconomic burden of fractures: today and in the 21st century. Am. J. Med. 103, S20–S26.
Jones, G., Nguyen, T., Sambrook, P., Kelly, P., Eisman, J.A., 1994. Progressive loss of bone in the femoral neck in elderly people: longitudinal findings from the Dubbo osteoporosis epidemiology study. BMJ 309, 691–695.
Juszczyk, M.M., Cristofolini, L., Viceconti, M., 2011. The human proximal femur behaves linearly elastic up to failure under physiological loading conditions. J. Biomech. 44, 2259–2266.
Kanis, J.A., Borgstrom, F., De Laet, C., Johansson, H., Johnell, O., Jonsson, B., Oden, A., Zethraeus, N., Pfleger, B., Khaltaev, N., 2005. Assessment of fracture risk. Osteoporos. Int. 16, 581–589.
Kaptoge, S., Benevolenskaya, L., Bhalla, A., Cannata, J., Boonen, S., Falch, J., Felsenberg, D., Finn, J., Nuti, R., Hoszowski, K.J.B., 2005. Low BMD is less predictive than reported falls for future limb fractures in women across Europe: results from the European Prospective Osteoporosis Study. Bone 36, 387–398.
Keller, T.S., 1994. Predicting the compressive mechanical behaviour of bone. J Blomechanics 29, 1159–1168.
Keyak, J.H., Falkinstein, Y., 2003. Comparison of in situ and in vitro CT scan-based finite element model predictions of proximal femoral fracture load. Med. Eng. Phys. 25, 781–787.
Keyak, J.H., Rossi, S.A., Jones, K.A., Skinner, H.B., 1997. Prediction of femoral fracture load using automated finite element modeling. J. Biomech. 31, 125–133.
Keyak, J., Sigurdsson, S., Karlsdottir, G., Oskarsdottir, D., Sigmarsdottir, A., Zhao, S., Kornak, J., Harris, T.B., Sigurdsson, G., Jonsson, B.Y., 2011. Male–female differences in the association between incident hip fracture and proximal femoral strength: a finite element analysis study. Bone 48, 1239–1245.
Kheirollahi, H., Luo, Y., 2015. Assessment of hip fracture risk using cross-section strain energy determined by QCT-based finite element modeling. BioMed Res. Int. 2015.
Kim, K., Brown, J., Kim, K., Choi, H., Kim, H., Rhee, Y., Lim, S.-K., 2011. Differences in femoral neck geometry associated with age and ethnicity. Osteoporos. Int. 22, 2165–2174.
Krogue, J.D., Cheng, K.V., Hwang, K.M., Toogood, P., Meinberg, E.G., Geiger, E.J., Zaid, M., McGill, K.C., Patel, R., Sohn, J.H., 2020. Automatic hip fracture identification and functional subclassification with deep learning. Radiology: Artif. Intell. 2, e190023.
LaCroix, A.Z., Beck, T.J., Cauley, J.A., Lewis, C.E., Bassford, T., Jackson, R., Wu, G., Chen, Z., 2010. Hip structural geometry and incidence of hip fracture in postmenopausal women: what does it add to conventional bone mineral density? Osteoporos. Int. 21, 919–929.

Lekadir, K., Noble, C., Hazrati-Marangalou, J., Hoogendoorn, C., van Rietbergen, B., Taylor, Z.A., Frangi, A.F., 2016. Patient-specific biomechanical modeling of bone strength using statistically-derived fabric tensors, 44, 234–246.
Liu, Y., Zhang, A., Wang, C., Yin, W., Wu, N., Chen, H., Chen, B., Han, Q., Wang, J., 2020. Biomechanical comparison between metal block and cement-screw techniques for the treatment of tibial bone defects in total knee arthroplasty based on finite element analysis. Comput. Biol. Med. 125, 104006.
Liu, J., Gao, Y., Niu, B., Xiu, J., Wang, H., Wang, Y., Yang, Y., 2021. Biomechanical analysis of a novel clavicular hook plate for the treatment of acromioclavicular joint dislocation: a finite element analysis. Comput. Biol. Med. 133, 104379.
Longo, U.G., Viganò, M., de Girolamo, L., Banfi, G., Salvatore, G., Denaro, V., 2022. Epidemiology and management of proximal femoral fractures in Italy between 2001 and 2016 in older adults: analysis of the national discharge registry. Int. J. Environ. Res. Publ. Health 19, 16985.
Lotz, J., Cheal, E., Hayes, W.C., 1991. Fracture prediction for the proximal femur using finite element models: part II—nonlinear analysis. J. Biomech. 113, 353–360.
Luo, Y., Yang, H., 2019b. Assessment of hip fracture risk by cross-sectional strain-energy derived from image-based beam model, 63, 48–53.
Luo, Y., Yang, H., 2019a. Comparison of femur stiffness measured from DXA and QCT for assessment of hip fracture risk. J. Bone Miner. Metab. 37, 342–350.
Mai, H.T., Tran, T.S., Ho-Le, T.P., Center, J.R., Eisman, J.A., Nguyen, T.V., 2019. Two-thirds of all fractures are not attributable to osteoporosis and advancing age: implications for fracture prevention. J. Clin. Endocrinol. Metabol. 104, 3514–3520.
Marco, M., Giner, E., Caeiro-Rey, J.R., Miguélez, M.H., Larraínzar-Garijo, R.J.C.m., biomedicine, p.i., 2019. Numerical modelling of hip fracture patterns in human femur, 173, 67–75.
Marks, R., Allegrante, J.P., MacKenzie, C.R., Lane, J.M., 2003. Hip fractures among the elderly: causes, consequences and control. Ageing Res. Rev. 2, 57–93.
Masahiko Bessho, I.O., Matsumoto, Takuya, Ohashi, Satoru, Matsuyama, Juntaro, Tobita, Kenji, Kaneko, Masako, Nakamura, Kozo, 2009. Prediction of proximal femur strength using a CT-based nonlinear finite element method: differences in predicted fracture load and site with changing load and boundary conditions. Bone 45, 226–231.
Michalski, A.S., Besler, B.A., Burt, L.A., Boyd, S.K., 2021. Opportunistic CT screening predicts individuals at risk of major osteoporotic fracture. Osteoporos. Int. 32, 1639–1649.
Miguel Marco, E.G., Caeiro-Rey, JoséRamón, Miguélez, MHenar, Larraínzar-Garijo, Ricardo, 2019. Numerical modelling of hip fracture patterns in human femur. Comput. Methods Progr. Biomed. 173.
Mohammadi, H., Pietruszczak, S., Quenneville, C., 2021. Numerical analysis of hip fracture due to a sideways fall. J. Mech. Behav. Biomed. Mater. 115, 104283.
Muller, A., Ruegsegger, E., Ruegsegger, P., 1989. Peripheral QCT: a low-risk procedure to identify women predisposed to osteoporosis. Phys. Med. Biol. 34, 741.
Munckhof, S.V.D., Zadpoor, A.A., 2014. How accurately can we predict the fracture load of the proximal femur using finite element models? Clin. BioMech. 40, 226–231.
Mundi, S., Pindiprolu, B., Simunovic, N., Bhandari, M., 2014. Similar mortality rates in hip fracture patients over the past 31 years: a systematic review of RCTs. Acta Orthop. 85, 54–59.
Nieves, J.W., Formica, C., Ruffing, J., Zion, M., Garrett, P., Lindsay, R., Cosman, F., 2005. Males have larger skeletal size and bone mass than females, despite comparable body size. J. Bone Miner. Res. 20, 529–535.
Nishiyama, Kyle K., G.e, S., Guy, Pierre, Cripton, Peter, Boyd, Steven K., 2007. Proximal femur bone strength estimated by a computationally fast finite element analysis in a sideways fall configuration. J. Biomech. 46, 1231–1236.
Orwig, D.L., Chan, J., Magaziner, J., 2006. Hip fracture and its consequences: differences between men and women. Orthopedic Clinics 37, 611–622.
Orwoll, E.S., Marshall, L.M., Nielson, C.M., Cummings, S.R., Lapidus, J., Cauley, J.A., Ensrud, K., Lane, N., Hoffmann, P.R., Kopperdahl, D.L., 2009. Finite element analysis of the proximal femur and hip fracture risk in older men. J. Bone Miner. Res. 24, 475–483.
Pedersen, A.B., Ehrenstein, V., Szépligeti, S.K., Lunde, A., Lagerros, Y.T., Westerlund, A., Tell, G.S., Sørensen, H.T., 2017. Thirty-five–year trends in first-time hospitalization for hip fracture, 1-year mortality, and the prognostic impact of comorbidity. Epidemiology 28, 898–905.
Pinilla, T.P., Boardman, K.C., Bouxsein, M.L., Myers, E.R., Hayes, W.C., 1996. Impact direction from a fall influences the failure load of the proximal femur as much as age-related bone loss. Calcif. Tissue Int. ume 58, 231–235.
Robinovitch, S., Hayes, W.C., McMahon, T., 1991. Prediction of Femoral Impact Forces in Falls on the Hip.
Rui Zhang, H.G., Fang, Juan, Gao, Zhenhai, Dong, Zhu, 2014. Prediction of proximal femoral fracture in sideways falls using nonlinear dynamic finite element analysis. J. Mech. Med. Biol. 14.
Schileo, E., T, F., Cristofolinia, L., Vicecontia, B.M., 2008. Subject-specific finite element models implementing a maximum principal strain criterion are able to estimate failure risk and fracture location on human femurs tested in vitro. J. Biomech. 41, 356–367.
Szulc, P., Marchand, F., Duboeuf, F., Delmas, P., 2000. Cross-sectional assessment of age-related bone loss in men: the MINOS study. Bone 26, 123–129.
Testi, D., Viceconti, M., Cappello, A., Gnudi, S., 2002. Prediction of hip fracture can be significantly improved by a single biomedical indicator. Ann. Biomed. Eng. 30, 801–807.
Wakao, N., Harada, A., Matsui, Y., Takemura, M., Shimokata, H., Mizuno, M., Ito, M., Matsuyama, Y., Ishiguro, N.J.M.e., physics, 2009. The effect of impact direction on the fracture load of osteoporotic proximal femurs, 31, 1134–1139.
Wod, M., 2008. Height estimation from skeletal remains. Student Thesis in Biological Anthropology. Institute of Biology, University of Southern Denmark.
Yang, S., Luo, Y., Yang, L., Dall'Ara, E., Eastell, R., Goertzen, A.L., McCloskey, E.V., Leslie, W.D., Lix, L.M.J.B., 2018. Comparison of femoral strength and fracture risk index derived from DXA-based finite element analysis for stratifying hip fracture risk: a cross-sectional study, 110, 386–391.
Yano, S., Matsuura, Y., Hagiwara, S., Nakamura, J., Kawarai, Y., Suzuki, T., Kanno, K., Shoda, J., Tsurumi, Y., Ohtori, S.J.B., 2022. Determinants of fracture type in the proximal femur: biomechanical study of fresh frozen cadavers and finite element models, 158, 116352.
Yoshikawa, T., Turner, C., Peacock, M., Slemenda, C., Weaver, C., Teegarden, D., Markwardt, P., Burr, D., 1994. Geometric structure of the femoral neck measured using dual-energy X-ray absorptiometry. J. Bone Miner. Res. 9, 1053–1064.
Yosibash, Z., Trabelsi, N., Buchnik, I., Myers, K.W., Salai, M., Eshed, I., Barash, Y., Klang, E., Tripto-Shkolnik, L., 2023. Hip fracture risk assessment in elderly and diabetic patients: combining autonomous finite element analysis and machine learning. J. Bone Miner. 38, 876–886.